Frontiers Special issue: Understanding Natural H_2 Systems - their Exploration and Stimulation

Title:

Low-temperature hydrogen production and consumption in partially-hydrated peridotites in Oman: implications for stimulated geological hydrogen production

Authors:

Alexis S. Templeton and Eric T. Ellison
Department of Geological Sciences, University of Colorado

Peter B. Kelemen and James Leong
Columbia University

Eric S. Boyd and Daniel R. Colman
Department of Microbiology and Cell Biology, Montana State University

Juerg M. Matter
University of Southampton

Keywords:

peridotite, hydrogen, serpentinization, microbial, stimulation

7. Supplementary Information

7.1 Construction of the Interactive Model and Interpretation of Figure 6

https://ericellison.shinyapps.io/gain_loss/

In order to assess the potential feasibility and profitability of stimulated geological H_2 production, we constructed a model that integrates the serpentinization rate and associated H_2 production of a stimulated reactive volume (SRV) of subsurface peridotite. We hypothesize that one of the main limits on the H_2 production rate in the subsurface is the reactive surface area that can be exposed to fluids. Studies have measured the rate of conversion of crushed minerals (e.g. olivine) and rocks (e.g. peridotite) to secondary products such as serpentine minerals in laboratory based hydrothermal experiments (e.g. Martin and Fyfe, 1970). Trends in these measured values are then extrapolated to lower temperatures (e.g. Kelemen and Matter, 2008). Based on simple assumptions of reactive surface area, the conversion rate for different grain sizes can also be inferred (e.g. Leong et al., 2023).

The basis for calculating conversion rates is that in the experiments, a reaction front penetrates into the grain, producing a fully reacted and inert rind on the reactant. The linear rate of penetration is a constant for any grain size at a fixed P,T and fluid composition, but that rate is a strong function of temperature. While the linear rate of penetration (e.g. mm/day) is constant, the actual volumetric rate of conversion (%/day) is then a decreasing function of grain size. Furthermore, as the grains react, the grain size of the unreacted core shrinks. This means that the reactive surface area shrinks, meaning the total reaction rate naturally diminishes over time. This is essentially a simple shrinking particle model, similar to those used in fluid-particle reaction kinetics (Homma et al., 2005; Fogler, 2016; Russo et al., 2020); here we ignore diffusion effects and focus on the effect of contracting reactive surface area on the reaction rate.

We constructed a model that accepts the following relevant inputs:

1. The penetration rate of the reaction front
2. The available Fe that will be reacted in the rock (assuming 100% yield to H_2)
3. The timeframe in which the system will operate.
4. The CapEx cost of the system
5. The ongoing OpEx cost of the system
6. The “grain size” of the rock system, which is the typical fracture spacing in the rock.
7. The dimensions of the total accessed/reacted volume of the system
8. The net sales price of H_2 produced
9. The initial bulk density of the rock

Based on these inputs, the model makes several calculations:

1. Using the dimensions of the reaction zone, the total volume of reacted rock is calculated (e.g. total volume = length x width x depth)
2. Using the total volume and the grain size, the number of reacted grains is calculated (e.g. number of grains = total volume / grain size)

3. Using the number of reacted grains, grain size, and the penetration rate of the reaction, and reaction time, the volume of rock that will actually participate in the reaction is calculated based on the shrinking particle model. The reacted volume is not allowed to exceed the total volume.
4. The reacted volume is converted to a reacted mass using the bulk density (e.g. reacted mass = reacted volume x bulk density)
5. The reacted mass and the concentration of available Fe is used to calculate the H_2 produced (e.g. reacted mass * kilograms of Fe per kilogram of rock * kilograms of H_2 per kilogram of Fe).
6. The value of the produced H_2 is calculated using the H_2 price (e.g. H_2 value = H_2 produced * H_2 price).
7. The total profit is calculated from the H_2 value and the capital expense (CapEx) and operating expense (OpEx) costs of the system (e.g. profit = H_2 value – CapEx – OpEx * time).

Once the model has been constructed, we are able to explore the larger parameter space, by adjusting values of each of the inputs. For example, **Figure 6** in the main text illustrates the results for a broad range of penetration rates and grain sizes, with the remaining input parameters fixed as shown in Supplementary Table 1.

Input Parameter	Value for Figure 6
Operation time	15 years
Fe(II) content available for reaction	4.5 wt% Fe(II)
Capital Expense cost of system (including drilling, site improvements, etc.)	\$600,000
Total depth of injection and production boreholes	800 m
Depth to H_2 stimulation zone	300 m
Distance between injection and production wells	100 m
Width of reaction zone	50 m
Sale price of H_2 (net of any purification and/or transportation costs)	\$5/kg
Initial rock density	2.7 g/cm^3
Operating Expense of system	\$200,000/yr

It is also possible to visualize H_2 production and economics as a function of time, illustrating the diminishing rate of H_2 production as the reactive surface area contracts. These subsidiary graphs can be viewed by clicking any location inside of a graph like the one shown in **Figure 6**.

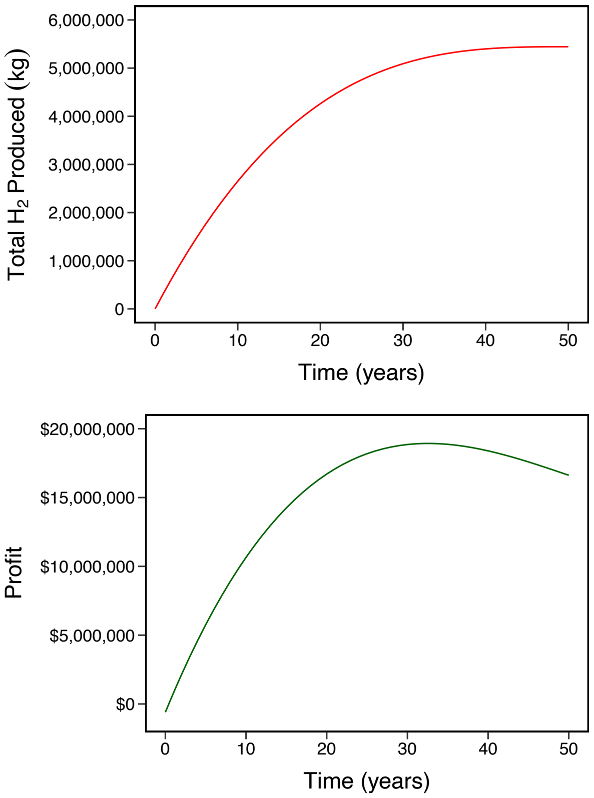

Supplemental Figure 1: Time evolution of H_2 production and system profit over 50 years. Input parameters as in SI Table 1, and with the penetration rate set to 10-12.5¬ and grain size = 1 mm. Note that we view this combination of rate and grain size as unrealistic, but it was chosen to emphasize the evolution of the system. After 33 years, the system begins losing money because operation expense exceeds the value of new H_2 produced.

6.2 Additional calculation of microbial H_2 consumption rates

To quantify predicted H_2 production through calculations that follow the approaches laid out in Hoehler et al. (2023) we need to know the energy requirement of the peridotite-hosted biosphere. We continue to use the average value of 10^5 anaerobic cells/cm^3 characterized so far in rocks and fluids recovered from the upper 400 meters of the peridotite aquifers. The turnover rate is unknown, so – as in Section 2.5 – we assume that the standing biomass replaces itself with one turnover per year. From this, the energy requirement can be estimated from the Hoehler et al. (2023) compilation as 0.001 Joules/sec/gC. Assuming mass of carbon in a cell is 30 femtograms (Amenabar 2017), this scales to $3x10^{-9}$gC/cm^3, yielding an energy requirement of $9.5*10^{-5}$ Joules/cm^3/yr, or $9.5*10^{10}$ J/km^3/yr.

If we use a calculated maximum of $2.393*10^{10}$ Joules produced per tonne of H_2 consumed in methanogenesis, calculated from the maximum ΔG of $H_2 + 4CO_2 \leftarrow\rightarrow CH_4 + 2H_2O$ under far from equilibrium conditions (Leong and Shock, 2020), this yields an estimate of 3.95 tonnes of H_2/km^3/yr.

6.3 Hydrogenase abundance

The community metagenomes were generated by filtering biomass from well/borehole waters and subjecting the biomass to DNA extraction and shotgun (meta)genome sequencing. Metagenomic sequence was assembled as we have described previously (Fones et al., 2019, 2021; Colman et al., 2022) and assembled sequence data was interrogated for genes encoding homologs of the large subunit of [NiFe]- and [FeFe]-hydrogenases using a combination of hidden Markov model (HMM) and BLAST-based approaches, as previously described (Søndergaard et al., 2016; Colman et al., 2017). Homologs from each class were aligned and examined for signature protein motifs as previously described (Peters et al., 2015) and were normalized as the number of homologs recovered per 1000 protein encoding genes that were sequenced within each metagenome. Additional information for hydrogenase sequences are provided in **Supp. Tables B2 and B3** (see separate Excel data sheets).

6.4 Supplementary Information References

Colman, D. R., Kraus, E. A., Thieringer, P. H., Rempfert, K., Templeton, A. S., Spear, J. R., et al. (2022). Deep-branching acetogens in serpentinized subsurface fluids of Oman. Proc. Natl. Acad. Sci. 119, e2206845119. doi: 10.1073/pnas.2206845119.

Colman, D. R., Poudel, S., Stamps, B. W., Boyd, E. S., and Spear, J. R. (2017). The deep, hot biosphere: Twenty-five years of retrospection. Proc. Natl. Acad. Sci. 114, 6895–6903. doi: 10.1073/pnas.1701266114.

Fogler, H. S. (2016). Elements of Chemical Reaction Engineering, 5th Edition. Available at: https://learning.oreilly.com/library/view/elements-of-chemical/9780133887822/ [Accessed November 18, 2023].

Fones, E. M., Colman, D. R., Kraus, E. A., Nothaft, D. B., Poudel, S., Rempfert, K. R., et al. (2019). Physiological adaptations to serpentinization in the Samail Ophiolite, Oman. ISME J. 13, 1750–1762. doi: 10.1038/s41396-019-0391-2.

Fones, E. M., Colman, D. R., Kraus, E. A., Stepanauskas, R., Templeton, A. S., Spear, J. R., et al. (2021). Diversification of methanogens into hyperalkaline serpentinizing environments through adaptations to minimize oxidant limitation. ISME J. 15, 1121–1135. doi: 10.1038/s41396-020-00838-1.

Hoehler, T. M., Mankel, D. J., Girguis, P. R., McCollom, T. M., Kiang, N. Y., and Jørgensen, B. B. (2023). The metabolic rate of the biosphere and its components. Proc. Natl. Acad. Sci. 120, e2303764120. doi: 10.1073/pnas.2303764120.

Homma, S., Ogata, S., Koga, J., and Matsumoto, S. (2005). Gas–solid reaction model for a shrinking spherical particle with unreacted shrinking core. Chem. Eng. Sci. 60, 4971–4980. doi: 10.1016/j.ces.2005.03.057.

Kelemen, P. B., and Matter, J. (2008). In situ carbonation of peridotite for CO2 storage. Proc. Natl. Acad. Sci. 105, 17295–17300. doi: 10.1073/pnas.0805794105.

Leong, J. A. M., and Shock, E. L. (2020). Thermodynamic constraints on the geochemistry of low-temperature, continental, serpentinization-generated fluids. Am. J. Sci. 320, 185–235. doi: 10.2475/03.2020.01.

Leong, J. A., Nielsen, M., McQueen, N., Karolytė, R., Hillegonds, D. J., Ballentine, C., et al. (2023). H2 and CH4 outgassing rates in the Samail ophiolite, Oman: Implications for low-temperature, continental serpentinization rates. Geochim. Cosmochim. Acta 347, 1–15. doi: 10.1016/j.gca.2023.02.008.

Martin, B., and Fyfe, W. S. (1970). Some experimental and theoretical observations on the kinetics of hydration reactions with particular reference to serpentinization. Chem. Geol. 6, 185–202. doi: 10.1016/0009-2541(70)90018-5.

Peters, J. W., Schut, G. J., Boyd, E. S., Mulder, D. W., Shepard, E. M., Broderick, J. B., et al. (2015). [FeFe]- and [NiFe]-hydrogenase diversity, mechanism, and maturation. Biochim. Biophys. Acta BBA - Mol. Cell Res. 1853, 1350–1369. doi: 10.1016/j.bbamcr.2014.11.021.

Russo, V., Grénman, H., Cogliano, T., Tesser, R., and Salmi, T. (2020). Advanced Shrinking Particle Model for Fluid-Reactive Solid Systems. Front. Chem. Eng. 2. Available at: https://www.frontiersin.org/articles/10.3389/fceng.2020.577505 [Accessed November 18, 2023].

Søndergaard, D., Pedersen, C. N. S., and Greening, C. (2016). HydDB: A web tool for hydrogenase classification and analysis. Sci. Rep. 6, 34212. doi: 10.1038/srep34212.